Journal of Materials Chemistry C

PAPER

View Article Online
View Journal

Cite this: DOI: 10.1039/c5tc03354c

Photophysical properties of push–pull 8-aryl-deoxyguanosine probes within duplex and G-quadruplex structures†

Darian J. M. Blanchard,[a] Kaila L. Fadock,[a] Michael Sproviero,[a] Prashant S. Deore,[a] Thomas Z. Cservenyi,[a] Richard A. Manderville,*[a] Purshotam Sharma[bc] and Stacey D. Wetmore*[b]

In this study, we outline the structural and photophysical properties of donor–acceptor (D–A) 8-aryl-2′-deoxyguanosine (8aryldG) probes within duplex and G-quadruplex (GQ) structures produced by the thrombin binding aptamer (TBA, 5′-GGTTG$_5$G$_6$TG$_8$TGGTTGG). The probes vary in 8-aryl ring size, degree of twist angle between the aryl ring and nucleobase component, degree of acceptor character, and nature of visibly emissive charge transfer (CT) states. Probes with the aryl ring directly attached to the nucleobase favor the *syn*-conformation and strongly destabilize the duplex structure, as measured by UV thermal melting experiments. However, these probes can stabilize the antiparallel GQ produced by TBA when inserted into the G-tetrad at the *syn*-G$_5$ position, and strongly decrease GQ stability when inserted at the *anti*-G$_6$ position. Nucleoside probes with the aryl ring separated from the nucleobase by a vinyl linker favor the *anti*-conformation. Furthermore, the nature of the aryl group dictates an ability of these probes to be accomodated within the GQ at the *anti*-G$_6$ position. 8AryldG probes that favor planar CT states (CT$_P$) exhibit bright emission in both duplex and GQ structures, but lack fluorescence sensitivity to changes in the microenvironment. In contrast, probes that afford twisted CT states (CT$_T$) exhibit weak fluorescence in duplex and GQ structures in water, but display fluorescence signalling capability for monitoring GQ formation in a crowded environment.

Received 15th October 2015,
Accepted 23rd November 2015

DOI: 10.1039/c5tc03354c

www.rsc.org/MaterialsC

Introduction

Fluorescence spectroscopy is a powerful bioanalytical tool for studying the structure and dynamics of biological macromolecules. Although proteins possess naturally fluorescent amino acids, purines and pyrimidines of nucleic acids are practically nonemissive and thus diverse approaches have been devised for base modification to generate fluorescent nucleobase analogs.[1–4] Effective fluorescent nucleobase mimics should not hamper Watson–Crick hydrogen bonding or the hybridization/folding of the native oligonucleotide and should be capable of clear fluorescence signalling.

A relatively simple and effective way to generate a fluorescence nucleobase probe is to attach a 5-membered heterocycle, such as furan or thiophene, to either the 5-position of a pyrimidine[5–8] or the 8-position of a purine.[9–13] The 5-modified pyrimidine analogs exhibit no impact on the *anti*-orientation or sugar pucker of the native nucleosides and behave like molecular rotors with emission that is sensitive to solvent viscosity.[7,8] In contrast, 8-substituted purines can shift the conformational equilibrium of the glycosidic bond from *anti* to *syn*.[14] The *syn*-preference of the 8-modified purines leads to significant decreases in thermal stability of the duplex compared to the unmodified helix.[9,15] Nevertheless, the 8-substituted purines exhibit emission that is sensitive to solvent polarity for predicting probe conformation in a duplex environment.[9] The 8-substituted 2′-deoxyguanosine (dG) derivatives are also particularly useful for monitoring G-quadruplex (GQ) folding by G-rich oligonucleotides.[10–13] Specifically, 8-furyl-dG (FurdG) stabilizes an antiparallel GQ structure when placed in a *syn*-position within the G-tetrad. The emission of FurdG at ~380 nm is quenched in the duplex, but lights-up in the GQ, and is accompanied by an energy-transfer peak at ~290 nm.[10–13] Fluorescent probes that can distinguish GQ structures from duplexes or single-strands are of vital importance because GQs are produced *in vivo*[16] and appear to play a critical role in gene regulation, chromosomal stability

[a] Department of Chemistry & Toxicology, University of Guelph, Guelph, ON, Canada N1G 2W1. E-mail: rmanderv@uoguelph.ca
[b] Department of Chemistry & Biochemistry, University of Lethbridge, Lethbridge, AB, Canada T1K 3M4
[c] Centre for Computational Sciences, Central University of Punjab, Bathinda, Punjab, 151001, India

† Electronic supplementary information (ESI) available: Computational details, Tables S1, S2 and Fig. S1–S4, NMR of phosphoramidites and MS analysis of mTBA oligonucleotides. See DOI: 10.1039/c5tc03354c

and telomerase activity.[17] Furthermore, a wide variety of DNA aptamers that bind specific ligands with high affinity and specificity produce GQ structures upon ligand binding.[18,19] General fluorescent approaches for detecting GQ formation include end-labelled fluorescent quench,[20] pyrene excimer assays,[21] and label-free dyes, such as thioflavin T (ThT)[22,23] and triphenylmethane (TPM).[24] The level of prescision offered by internal placement of a fluorescent nucleobase analog should complement these approaches,[13] especially in aptamer detection strategies where the internal probe may assist in establishing Gs in the tetrad *versus* loop positions, site(s) of ligand binding, and for removing false negatives or positives that can occur with the use of external dyes that are not covalently attached to the aptamer.[23]

While purines and pyrimidines containing conjugated 5-membered heterocycles have proven to be useful fluorescent surrogates, they lack visible emission and the 5-modified pyrimidines suffer from low quantum efficiency (Φ = 0.01–0.035).[5–8] Efforts to improve the photophysical features of the pyrimidine analogs have produced new visibly emissive derivatives exhibiting donor–acceptor (D–A) characteristics.[25–27] Such a push–pull fluorescent cytidine derivative has proven particularly valuable for monitoring i-motif-duplex exchange.[28]

We present here the utility of visibly emissive 8-aryl-dG derivatives for monitoring antiparallel GQ formation by the thrombin binding aptamer (TBA).[29] This 15mer DNA oligonucleotide (5′-GGTTGGTGTGGTTGG-3′) is the most commonly used model system to demonstrate proof-of-concept for probe performance in an GQ-based aptamer.[30] Push–pull dG analogs are prepared by either attaching electron-deficient aryl groups to the 8-position of the electron-rich dG nucleobase,[10,31–34] or by expanding the conjugation of the 8-aryl ring system. For push–pull biphenyl systems, the nature of visibly emissive charge transfer (CT) states (planar *versus* twisted) depends on steric hindrance to planarity and the degree of D–A character.[35,36] Such D–A biphenyls can exhibit large Stokes shifts coupled with significant changes in emission wavelength in response to solvent polarity. Thus, compared to FurdG that only displays changes in emission intensity upon GQ formation,[10–13] it was anticipated that D–A 8aryldG probes might also exhibit changes in emission wavelength and thereby result in more efficient fluorescent probes for GQ detection.

In our studies, four probes (AcphdG, BthdG, QdG and PydG, Fig. 1) contain an aryl ring directly attached to the 8-position of dG and vary in aryl ring size, degree of twist between the aryl ring and dG component (defined by θ, Fig. 1) and degree of acceptor character. The structural and optical properties of 8-benzo[*b*]thienyl-dG (BthdG),[9] 8-quinolyl-dG (QdG)[15] and 8-(pyren-1-yl)-dG (PydG)[37,38] have previously been examined in a DNA duplex environment and each probe exhibits fluorescence in the single-strand that is sensitive to hybridization. However, none of the probes have been tested in a GQ-folding oligonucleotide, such as TBA. For the AcphdG and BthdG derivatives, probe performance was also compared to the vAcphdG and vBthdG analogs, in which the acetylphenyl (Acph) and benzo[*b*]thienyl (Bth) groups are separated from the dG component by a vinyl linker to increase conjugation. 8-Vinyl-aryldG derivatives can be useful for monitoring GQ-duplex exchange by exhibiting an increase in emission intensity upon GQ formation due to effective energy transfer from the unmodified guanines in the G-tetrad.[39] Our studies highlight the fluorescent properties of D–A 8aryldG analogs that may have the potential to serve as effective internal probes in biosensing applications.

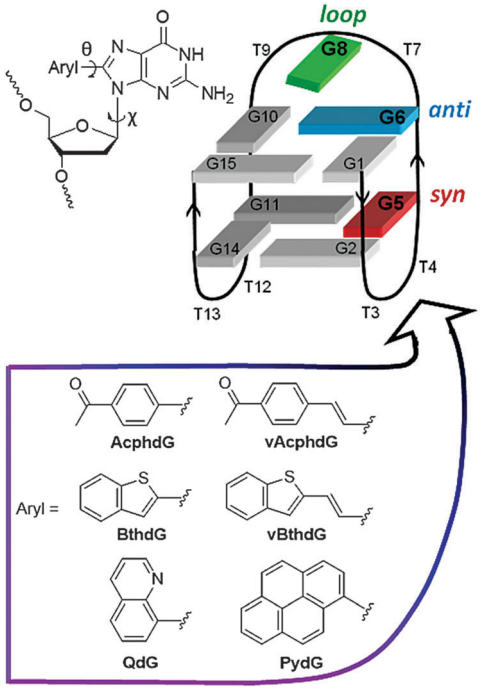

Fig. 1 Structures of 8aryldG probes and sites of incorporation into TBA G-tetrad; (G5, red, *syn*), (G6, blue, *anti*), and loop region (G8, green). The dihedral angle χ ($\angle$(O4′–C1′–N9–C4)) defines the glycosidic bond orientation to be *anti* (χ = 180 ± 90°) or *syn* (χ = 0 ± 90°), and θ ($\angle$(N9–C8–C10–X11)) defines the degree of twist between the nucleobase and the 8-substituent.

Results and discussion

Nucleoside properties

The synthesis of various 8aryldG probes with an aryl ring directly attached to the 8-position of dG (*i.e.*, AcphdG, BthdG,[9] QdG[15] and PydG,[38] Fig. 1) has been reported previously by our laboratory. Synthesis is facilitated using a palladium-catalyzed Suzuki–Miyaura cross-coupling reaction between 8-Br-dG[40] and the appropriate boronic acids in basic water–MeCN mixtures, as outlined by Western and coworkers.[41] This procedure was also employed to prepare the vinyl derivatives.[13] However, for these analogs the requisite boronic acids were not commercially available, and were synthesized starting from 4-bromo-acetylbenzene and 2-bromo-benzo[*b*]thiophene (Scheme 1). First, the ethynylarene derivatives were obtained by a Sonogashira coupling of the bromoarenes with (trimethylsilyl)acetylene (TMSA),[42] which was followed by basic removal of the TMS group.[43] A Cu-catalyzed hydroboration of the ethynylarenes in the presence of bis(pinacolato)diboron produced the

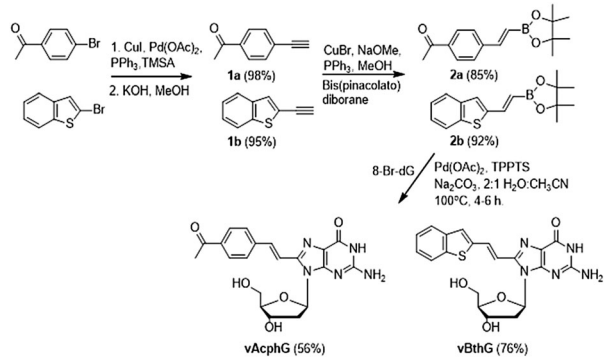

Scheme 1 Synthesis of vAcphdG and vBthdG.

desired boronic esters[44] for subsequent Pd-catalyzed coupling to 8-Br-dG.[13]

The *syn–anti* conformation of the nucleoside probes in DMSO was examined using ^{1}H and ^{13}C-NMR spectroscopy. A conformational shift from *anti* to *syn* correlates with a downfield shift of the H2′, C1′, C3′ and C4′ signals and an upfield shift of the C2′ signal, compared to the signals observed for native dG.[9,39] According to this analysis (Table S1, ESI†), AcphdG, BthdG, QdG and PydG adopt the *syn*-conformation in DMSO, while the two vinyl derivatives (vAcphdG and vBthdG) adopt the *anti*-conformation. The vinyl protons for vAcPhdG and vBthdG in DMSO showed coupling constants (J) of 16 Hz, which is consistent with the *E*-isomer, while J values of ~12 Hz have been reported for the *Z*-isomer of related 8vinylaryldG derivatives.[45]

The structural and electronic features of the nucleoside probes were also examined by DFT calculations, as presented previously for BthdG[9] and QdG.[15] In the gas-phase, all nucleoside probes favor the *syn*-conformation by 15.9–29.5 kJ mol^{-1} (Fig. 2 and Table 1) and benefit from an intramolecular O5′-H···N3 H-bond. For probes with the aryl ring directly attached

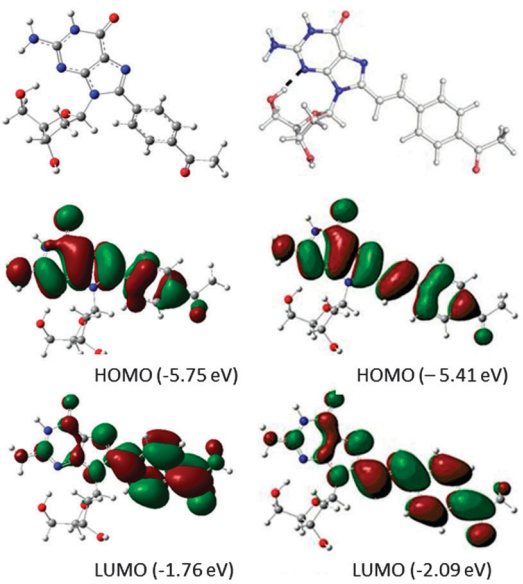

Fig. 2 Ground-state B3LYP/6-31G(d) global minima and orbital density plots of AcphdG and vAcphdG.

Table 1 Structural and electronic properties of 8aryldG probes

Probe[a]	E_{anti}–E_{syn}	χ/θ	μ_g	HOMO	LUMO	ΔE_{calcd}
BthdG	24.5	66.8/211.1	5.5	−5.51	−1.33	4.18
AcphdG	26.0	67.2/38.8	5.8	−5.75	−1.76	3.99
QdG	29.5	52.2/305.6	4.3	−5.49	−1.77	3.72
PydG	20.9	61.1/58.8	4.9	−5.29	−1.70	3.59
vBthdG	17.4	54.8/181.6	4.3	−5.18	−1.80	3.38
vAcphdG	15.9	55.0/181.9	5.5	−5.41	−2.08	3.33

[a] E_{anti}–E_{syn} in kJ mol^{-1}; χ/θ in degrees; μ_g in Debye; HOMO/LUMO and ΔE_{calcd} (HOMO–LUMO gap) in eV. Data for BthdG is taken from ref. 9.

to the 8-site of dG, the order of the E_{anti}–E_{syn} energy difference (QdG > AcphdG > BthdG > PydG) was unexpected as the bulkiest PydG exhibited the smallest *syn*-preference. Interestingly, insertion of the vinyl linker decreased the *syn*-preference by 10.1 kJ mol^{-1} for vAcphdG (15.9 kJ mol^{-1} compared to 26.0 kJ mol^{-1} for AcphdG), but only by 7.1 kJ mol^{-1} for vBthdG (17.4 kJ mol^{-1} compared to 24.5 kJ mol^{-1} for BthdG). The twist about the aryl ring-nucleobase linker (as defined by θ, see Fig. 1) was PydG (58.8°) > QdG (54.4°) > AcphdG (38.8°) > BthdG (31.1°), while the two vinyl derivatives are essentially planar with vAcphdG (1.9°) > vBthdG (1.6°). The vinyl derivatives also possess the lowest calculated HOMO–LUMO gap (ΔE_{calcd}), followed by PydG < QdG < AcphdG < BthdG. Orbital density plots for AcphdG and vAcphdG (Fig. 2) highlight the push–pull character of the probes, as the LUMO of both probes exhibits greater density on the 8-aryl ring system.[10,31]

Photophysical parameters of the nucleoside probes are given in Table 2. Absorption spectra of BthdG, AcphdG, vBthdG and vAcphdG in aqueous buffer (Fig. S1, ESI†) showed both planar and nonplanar conformations. The absorption at ~290 nm was ascribed to the nonplanar twisted state, while planar states for AcphdG and BthdG occur at 315 nm. Planar absorptions were at ~375 nm for the vinyl derivatives. The vAcphdG probe exhibited dual fluorescence in water, with wavelengths dependent on the excitation maxima (Fig. 3). Excitation of the twisted conformation at 290 nm produced emission at 409 nm and 585 nm (purple trace, Fig. 3B), while excitation of the planar conformation at 375 nm afforded emission at 488 nm and 585 nm (green trace, Fig. 3B). The blue-shifted emission peak at 409 nm was ascribed to a "locally excited" (LE) state, while the peaks at 488 and 585 nm were ascribed to charge transfer (CT) states. The most red-shifted 585 nm CT peak stemming from

Table 2 Spectroscopic properties of 8-aryl-dG probes

Probe[a]	λ_{max} H_2O	λ_{em} (Φ_{fl}) H_2O	λ_{em} (Φ_{fl}) CH_3CN	λ_{em} (Φ_{fl}) $CHCl_3$	$\varepsilon_{\lambda_{max}} \times \Phi_{fl}$ H_2O
BthdG	315	419 (0.46)	413 (0.60)	405 (0.25)	8570
AcphdG	283	419 (0.006)	498 (0.13)	467 (0.23)	80
QdG	313	407 (0.03)	510 (0.05)	468 (0.19)	240
PydG	342	397 (0.09)	476 (0.27)	435 (0.30)	2015
vBthdG	377	473 (0.29)	470 (0.41)	459 (0.25)	17 900
vAcphdG	375	488 (0.03)	526 (0.09)	488 (0.17)	870

[a] λ values in nm; fluorescence quantum yields are relative to quinine bisulfate (Φ_{fl} = 0.546 in 0.5 M H_2SO_4); brightness factor is $\varepsilon_{\lambda_{max}} \times \Phi_{fl}$.

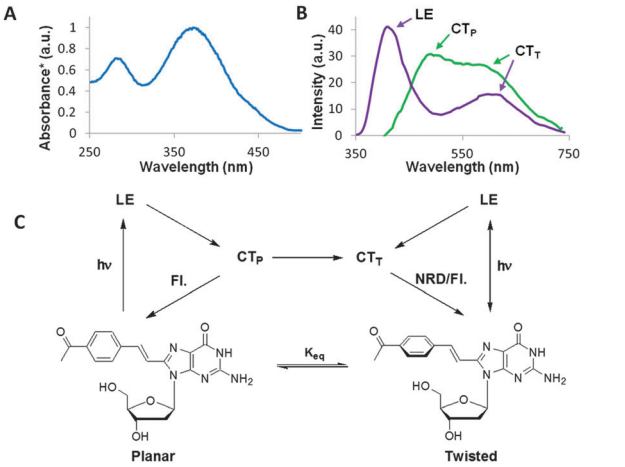

Fig. 3 UV absorption (A) and emission spectra (B) of vAcphG in H_2O with accompanying schematic (C) for the different emissive states; NRD = nonradiative decay.

excitation of the twisted structure was assigned to a TICT (twisted intramolecular CT, *i.e.* CT_T) state, while the emission at 488 nm was ascribed to a planar delocalized CT state (CT_P). The CT_T state results from relative rotation of the donor and acceptor groups, leading to decoupling of the orbital. This allows for an electron transfer from the donor to the acceptor, producing a twisted biradicaloid species with a large dipole. The vAcphdG probe was weakly emissive in H_2O (Table 2), as TICT states are strongly quenched in polar protic solvents.[35,36] The probe exhibited stronger emission in $CHCl_3$ (Φ_{fl} = 0.17) at 488 nm (Table 2), which was ascribed to the CT_p state.

The benzo[*b*]thienyl group in BthdG is not a strong enough acceptor to generate CT states, and bright LE emission at 419 nm (Φ_{fl} = 0.46) in H_2O was observed.[9] The Acph group is a stronger acceptor than Bth and generates emissive CT states in both CH_3CN and $CHCl_3$ (Table 2). Thus, we propose that excitation of AcphdG results in a biradicaloid CT_T state being readily populated, which is not emissive in water due to dynamic quenching. Therefore, locally excited (LE) emission is observed at 419 nm (Φ_{fl} = 0.006) in H_2O, which is attributed to the relatively small population of excited state AcphdG that did not undergo CT processes and equilibrate to the lower energy CT_T state. Similar emissive features were observed for QdG,[15] while the PydG probe gave dual emission in H_2O at 397 nm (LE) and 482 nm (CT). Interestingly, vBthdG gave only CT emission at ~473 nm in all three solvents regardless of the excitation maxima (290 nm *versus* 377 nm); the intensity of the CT state in H_2O (Φ_{fl} = 0.29) suggested formation of a planar CT_P state. Overall, the AcphdG, QdG, and vAcphdG probes containing the strongest acceptor groups provided the weakest fluorescence in H_2O due to their tendency to produce CT_T states. However, these probes exhibited strong emission sensitivity to solvent polarity. For example, vAcphdG provided emission at 584 nm in H_2O that shifted to 488 nm in $CHCl_3$ for a $\Delta\lambda_{em}$ of 96 nm.

Push–pull pyrimidine analogs exhibit fluorescence that is sensitive to solvent viscosity. For such analogs, a non-emissive rotational decay process from twisted excited states is expected to decrease emission intensity.[7,8] Increased solvent viscosity hinders formation of a twisted excited state, thereby increasing emission intensity. The D–A 8aryldG nucleosides (AcphdG, QdG, PydG, vBthdG and vAcphdG) also exhibited increased emission intensity with increased solvent viscosity (Table S2, ESI†). The two acetylphenyl derivatives (AcphdG and vAcphdG) were particularly sensitive to viscosity, displaying a 35- and 50-fold increase in emission intensity upon changing the solvent from water to 80% glycerol : 20% water. This was contrasted by the emissive behavior of BthdG, which displayed a 4-fold reduction in emission intensity from buffered water to 80% glycerol.[9]

Probe impact on GQ and duplex formation

To test the performance of the various 8aryldG probes in a GQ-folding oligonucleotide, the nucleoside probes were first converted into phosphoramidites for solid-phase oligonucleotide synthesis (see ESI† for synthetic details and NMR spectra of compounds). The GQ-folding TBA was chosen as the oligonucleotide substrate in order to make a direct comparison of the D–A probes in the current study to the previously reported properties of FurdG within TBA.[10] Thus, the probes were incorporated into the G_5 (*syn*-G) or G_6 (*anti*-G) positions of the G-tetrad, or G_8 of the TGT loop, of TBA (Fig. 1). The modified TBA (mTBA) oligonucleotides (see ESI† for UV-vis spectra and MS analysis) were initially studied using UV-thermal melting parameters (T_m values) and circular dichroism (CD) spectra to determine the impact of the 8aryldG probes on duplex and GQ stability and structure.

UV thermal melting studies

With the exception of vAcphdG, which exhibits the smallest E_{anti}–E_{syn} energy difference (Table 1), the 8aryldG probes strongly decreased duplex stability (T_m, Table 3). For the derivatives with the aryl ring directly attached to the dG nucleobase, the degree of destabilization correlated with the size of the 8-aryl group with AcphdG < BthdG < QdG ≈ PydG. Within this series of probes, it was also noted that insertion at position G_8 with the probe flanked by thymidines was more destabilizing than insertion at positions G_5 and G_6 with the probe flanked by a guanine. For the vinyl derivatives, it was surprising that vBthdG was strongly destabilizing within the duplex, given the *anti*-preference of the free nucleoside in DMSO (Table S1, ESI†). In fact, the vBthdG probe was more destabilizing than BthdG, which has a stronger *syn*-preference (Table 1). This suggested that the lipophilicity of the vBth moiety (vBthdG has a smaller dipole moment than BthdG, Table 1) may play a significant role in the observed destabilization.

In the GQ structures, AcphdG and BthdG stabilized the GQ at position *syn*-G_5 (ΔT_m = 6.9 and 1.9), but strongly decreased stability at *anti*-G_6 (ΔT_m = −20.2 and −23.3) due to the *syn*-preference of the 8aryldG base. Compared to FurdG,[10] both probes were not as stabilizing at G_5 (ΔT_m = 9.1 for FurdG) and were more destabilizing at G_6 (ΔT_m = −11 for FurdG) due to the increased ring size of Acph and Bth compared to Fur. Within the loop (G_8), both BthdG (ΔT_m = −8.1) and AcphdG (ΔT_m = −7.2)

Table 3 UV-thermal melting parameters for TBA oligonucleotides

Probe[a]	Site	T_m (D) (ΔT_m)	T_m (GQ) (ΔT_m)
dG	—	64.5	53.3
BthdG	5	55.0 (−9.5)	55.2 (1.9)
	6	55.5 (−9.0)	30.0 (−23.3)
	8	54.6 (−9.9)	45.2 (−8.1)
AcphdG	5	56.4 (−8.1)	60.2 (6.9)
	6	57.1 (−7.4)	33.1 (−20.2)
	8	56.3 (−8.2)	46.1 (−7.2)
QdG	5	50.6 (−13.9)	51.7 (−1.7)
	6	50.8 (−13.7)	No T_m
	8	48.2 (−16.3)	46.9 (−6.4)
PydG	5	52.0 (−12.5)	38.0 (−15.3)
	8	49.0 (−15.5)	31.2 (−22.1)
vBthdG	5	50.1 (−14.4)	51.6 (−1.7)
	6	54.1 (−10.4)	42.4 (−10.9)
	8	50.3 (−14.2)	50.4 (−2.9)
vAcphdG	5	60.1 (−4.4)	51.0 (−2.3)
	6	61.3 (−3.2)	55.9 (2.6)
	8	61.2 (−3.3)	50.4 (−2.9)

[a] T_m values (°C) of duplexes (D, 6.0 μM) measured in 100 mM sodium phosphate buffer pH 7.0 with 0.1 M NaCl, $\Delta T_m = T_m$ (mTBA D) − T_m (TBA D); T_m values of GQ (6.0 μM) in 100 mM potassium phosphate buffer pH 7.0 with 0.1 M KCl, $\Delta T_m = T_m$ (mTBA GQ) − T_m (TBA GQ); absorbance was monitored at 260 nm for Ds, 295 nm for GQs, with a heating rate of 1 °C min^{-1}, 5 ramps were conducted and all values are reproducible within 3%.

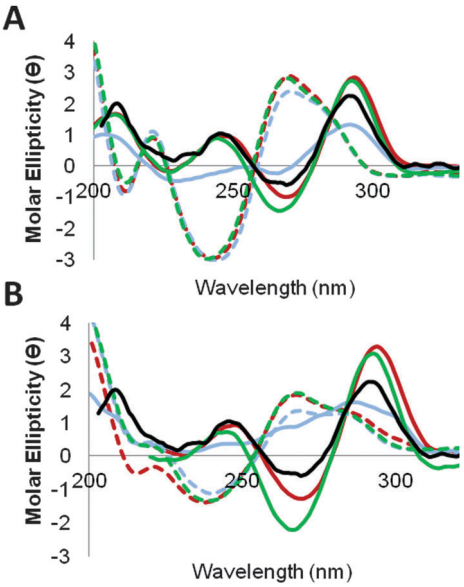

Fig. 4 CD spectral overlays of duplex (dashed lines) and GQ (solid lines) produced by (A) AcphdG-mTBA and (B) BthdG-mTBA; red lines (*syn*-G_5), blue lines (*anti*-G_6) and green lines (loop-G_8); black trace is GQ spectrum of unmodified TBA.

were not as destabilizing as the smaller FurdG probe ($\Delta T_m = -9.5$) due to increased stacking interactions for the larger probes in the loop-position. Thus, it was anticipated that QdG and PydG may exhibit a stabilizing influence in the loop-G_8 position through enhanced stacking interactions with the G-tetrad. The QdG probe was slightly destabilizing at *syn*-G_5, inhibited GQ folding at *anti*-G_6, and exhibited as slight increase in stability at G_8 compared to AcphdG. The PydG probe was only inserted into the G_5 and G_8 positions, where it strongly decreased the T_m value of the GQ structure.

The two vinyl derivatives exhibited similar T_m values at positions G_5 and G_8 within the GQ and were slightly destabilizing compared to the unmodified TBA. However, vBthdG had a significant destabilizing influence at *anti*-G_6 ($\Delta T_m = -10.9$), while vAcphdG exhibited a stabilizing influence ($\Delta T_m = 2.6$). A rationale for this difference in stability at G_6 may be the increased *syn*-preference of vBthdG compared to vAcphdG (Table 1) combined with increased lipophilicity of the vBth group (vBthdG has a smaller dipole moment than vAcphG, Table 1).

Circular dichroism

The mTBA duplexes and GQ structures were analysed using CD spectroscopy to determine probe impact on global tertiary structure. Representative spectra are shown in Fig. 4 for AcphdG-mTBA and BthdG-mTBA, while CD spectra for the other mTBA samples are available in the ESI† (Fig. S2). The duplexes showed B-DNA helix characteristics, with positive and negative sigmoidal CD curves and a crossover at ~260 nm.[46]

The antiparallel chair-type GQ of TBA exhibits a CD spectrum with a positive 295 nm peak, a smaller negative 265 nm peak, and a smaller positive peak at 245 nm (black trace in Fig. 4).[47] At positions *syn*-G_5 and loop-G_8, both AcphdG and BthdG produced CD spectra characteristic of the antiparallel GQ produced by unmodified TBA. However, at *anti*-G_6, BthdG produced a CD spectrum lacking the characteristic features of the GQ produced by TBA, suggesting that the probe inhibited antiparallel GQ formation (Fig. 4B, solid blue trace). At *anti*-G_6, AcphdG decreased the amplitudes of the positive and negative peaks (blue trace, Fig. 4A).

Fluorescence

The photophysical properties of the mTBA oligonucleotides (duplex (D) *vs.* GQ) are summarized in Table 4. A dominant feature of the D–A probes was the lack of significant emission intensity changes between duplex and GQ structures (I_{rel} values). The FurdG probe studied previously displayed I_{rel} values of ~10–60,[10] while the largest positive I_{rel} was 2.0 for AcphdG at *anti*-G_6 where the probe significantly decreased GQ stability (Table 3). In terms of wavelength changes, the two probes containing the Acph acceptor (AcphdG and vAcphdG) exhibited the largest $\Delta\lambda_{em}$ values (17–55 nm), which shifted to the blue upon GQ formation. Compared to FurdG within TBA,[10] the D–A probes exhibited fluorescence that was much more sensitive to probe position within TBA. For example, both AcphdG and QdG exhibited quenched emission at *syn*-G_5 in both duplex and GQ structures. However, in the loop-G_8 position, both probes displayed an increase in emission intensity in the duplex (8–10-fold increase compared to *syn*-G_5) that shifted to the red by 49 and 98 nm, respectively. For these probes, it is predicted that the CT_T state is quenched when the probe is flanked by an electron-rich G nucleobase due to electron-transfer from G. At the loop-G_8 position, the probes are flanked by two T residues in the duplex. In the GQ structure, the loop-G_8 probes can stack with the G-tetrad, and consequently both probes show

Table 4 Photophysical parameters of mTBA oligonucleotides

Probe[a]	Site	λ_{ex} (D)	λ_{em} (D) (I_{em})	λ_{ex} (GQ) ($\Delta\lambda_{ex}$)	λ_{em} (GQ) ($\Delta\lambda_{em}$, I_{rel})
BthdG	5	345	419 (375)	327 (−18)	419 (0, 1.3)
	6	334	423 (251)	338 (4)	420 (−3, 1.4)
	8	343	421 (431)	327 (−16)	416 (−5, 0.4)
AcphdG	5	343	494 (3)	330 (−13)	439 (−55, 1.7)
	6	333	507 (2)	341 (8)	480 (−27, 2.0)
	8	348	543 (20)	341 (−7)	496 (−47, 0.7)
QdG	5	325	382 (5)	315 (−10)	381 (−1, 1.4)
	8	327	480 (39)	328 (1)	496 (16, 0.3)
PydG	5	377	458 (674)	357 (−20)	464 (6, 0.9)
	8	368	458 (732)	361 (−7)	457 (−1, 0.8)
vBthdG	5	385	470 (999)	380 (−5)	471 (1, 0.6)
	6	390	467 (427)	388 (−2)	471 (4, 1.4)
	8	391	475 (756)	387 (−4)	470 (−5, 0.5)
vAcphdG	5	386	585 (19)	384 (−2)	559 (−26, 1.2)
	6	390	585 (33)	382 (−8)	565 (−20, 0.9)
	8	390	585 (22)	387 (−3)	568 (−17, 1.1)

[a] Excitation (λ_{ex}) and emission (λ_{em}) wavelengths in nm. Duplexes (d, 6.0 μM) measured (5 nm slit-width) in 100 mM sodium phosphate buffer pH 7.0 with 0.1 M NaCl, GQ (6.0 μM) in 100 mM potassium phosphate buffer pH 7.0 with 0.1 M KCl, $\Delta\lambda_{ex} = \lambda_{ex}$ (GQ) − λ_{ex} (D), $\Delta\lambda_{em} = \lambda_{em}$ (GQ) − λ_{em} (D), I_{rel} = emission intensity (I_{em}) (GQ)/I_{em}(D).

quenched emission in the GQ (I_{rel} = 0.7 and 0.3). The two brightest probes were PydG and vBthdG, which generate CT_P states. However, both probes exhibited minor changes in wavelength and emission intensity between duplex and GQ structures.

Representative emission spectra for the probes containing the Acph and Bth acceptor groups are shown in Fig. 5. At position *syn*-G_5 (Fig. 5A), the vAcphdG probe is significantly more emissive than AcphdG, showing a 5-fold increase in emission intensity with a ~100 nm wavelength shift to the red. However, at the loop-G_8 position (Fig. 5B), the AcphdG probe exhibited comparable emission intensity and wavelength to that of vAcphdG and is more useful for distinguishing duplex from GQ structures. Here, vAcphdG exhibits a slight increase in emission intensity upon GQ formation (I_{rel} = 1.2) that is accompanied by a 26 nm wavelength shift. In contrast, AcphdG provides visible emission in the duplex at 542 nm that is quenched (I_{rel} = 0.7) in the GQ structure with a wavelength change of 47 nm. Thus, AcphdG is useful for monitoring duplex-GQ exchange at the loop-G_8 position, while vAcphdG is not particularly useful because the probe does not exhibit strong emission signalling between the two topologies. An advantage for the vAcphdG probe is that it does provide visible emission following excitation at ~390 nm in all sites and can be placed at both *anti*- and *syn*-G positions with the G-tetrad. For the Bth acceptor probes (Fig. 5C), vBthdG is significantly brighter in the duplex than BthdG at *syn*-G_5, and exhibits greater change in emission intensity upon GQ formation. Overall, vBthdG is a much more useful probe than BthdG because it provides relatively bright visible emission in both duplex and GQ structures at ~470 nm following excitation at ~390 nm. However, a drawback to the vBthdG probe is its inability to be inserted into the *anti*-G_6 position without decreasing GQ stability (Table 3).

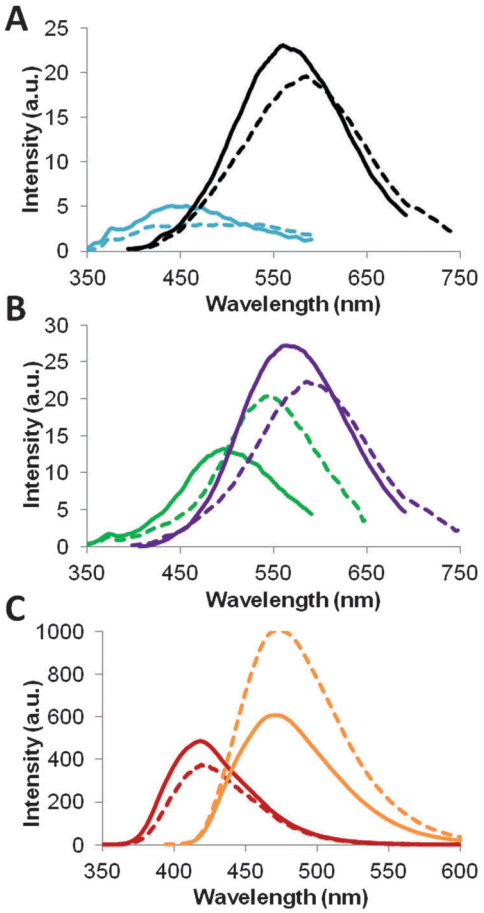

Fig. 5 Emission spectral overlays of duplex (dashed lines) and GQ (solid lines) produced by (A) AcphdG (blue lines) *vs.* vAcphdG (black lines) at *syn*-G_5, (B) AcphdG (green lines) *vs.* vAcphdG (purple lines) at loop-G_8 and (C) BthdG (red lines) *vs.* vBthdG (orange lines) at *syn*-G_5.

Probe performance induced by osmotic stress and molecular crowding

Given that the D–A nucleobase probes (especially AcphdG and vAcphdG) exhibit fluorescence that responds to changes in solvent polarity (Table 2) and viscosity (Table S2, ESI†), the emissive response of AcphdG- and vAcphdG-mTBA to changes in osmotic stress and molecular crowding conditions were examined (Fig. 6). To influence hydration conditions using osmotic stress, the water activity is typically changed by the addition of small neutral organic compounds, such as CH_3CN.[48] The large polymeric polyethylene glycols (PEGs) have been argued to promote macromolecular crowding and serve as effective reagents to mimic the intracellular environment.[49] Given the potential utility of internal fluorescent probes in construction of DNA nanodevices and DNA nanostructures, probe performance under alternative solvent or crowded conditions are important to establish.[50] Thus, the emission of the Acph-containing mTBA GQ structures in aqueous K^+ solution in the absence (Fig. 6, solid traces) and presence of 42.5% (v/v) CH_3CN (dotted traces), 42.5% (v/v) PEG-200 (dashed traces) and 42.5% (v/v) PEG-600 (long dashed traces) were determined.

At the *syn*-G_5 position (Fig. 6A), the GQ structure of AcphdG-mTBA exhibited quenched emission in aqueous K^+ solution.

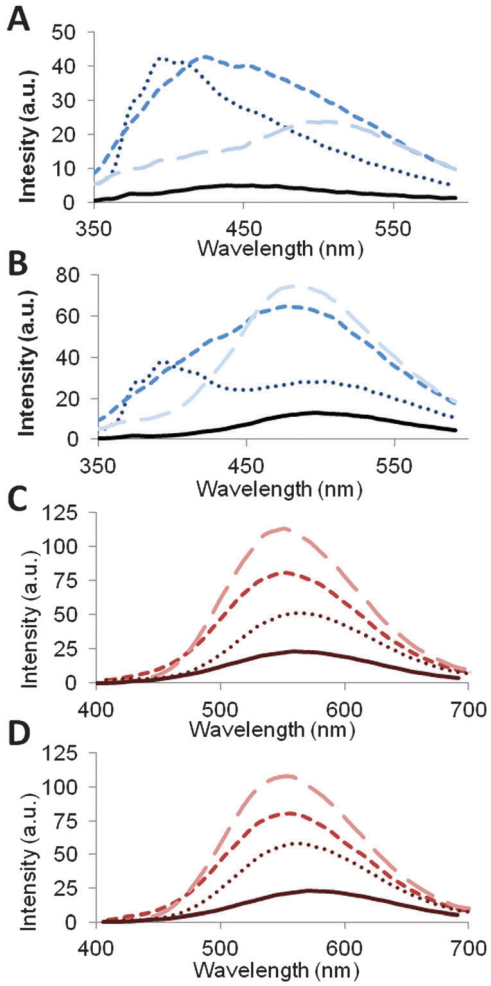

Fig. 6 Emission spectral overlays of AcphdG-mTBA (A and B) and vAcphdG-TBA (C and D) at *syn*-G_5 (A and C) and loop-G_8 (B and D) in K^+ solution (solid traces) and in the presence of 42.5% (v/v) CH_3CN (dotted traces), PEG-200 (dashed traces) and PEG-600 (long dashed traces).

In the presence of CH_3CN (dotted trace, Fig. 6A), the emission peaked at 396 nm for LE emission and displayed a 14-fold increase in intensity compared to the emission in water. In the presence of PEG-600 (long dashed trace), the emission peaked at 507 nm for CT emission and displayed an 8-fold intensity increase compared to the water emission. At the loop-G_8 position (Fig. 6B), the GQ structure of AcphdG-mTBA displayed CT emission at 496 nm. In the presence of CH_3CN, dual emission was observed with λ_{max} = 396 nm for an intensity increase of ~30-fold. In the presence of PEG-600, only CT emission was observed at 485 nm that displayed a 6-fold intensity increase compared to the emission of the GQ in water. In contrast, the emission response of vAcphdG-mTBA to the various additives was much more uniform (Fig. 6C and D). The probe exhibited a single emission band at ~560 nm that displayed an increase in intensity with water < CH_3CN < PEG-200 < PEG-600 at both *syn*-G_5 and loop-G_8; PEG-600 caused a 10-fold increase in intensity and 10 nm blue-shift in wavelength compared to the CT emission in water.

The viscosity-sensitive emissive response of the two push–pull probes in mTBA can be related to the behaviour of more typical fluorescent molecular rotors.[51] The AcphdG probe with the Acph moiety directly attached to the dG nucleobase resembled the behaviour 1,4-dimethylamino benzonitrile (DMABN), which displays photon emission from both LE and CT states. This indicates that the TICT energy gap is only slightly smaller than the LE energy gap. For these types of molecular rotors, the TICT formation rate, that depends on viscosity and solvent polarity, is the dominant factor that determines the relative intensity of the two emission bands.[51] Thus, the AcphdG probe showed complex patterns of dual emission upon addition of the various additives that was highly dependent on probe position (G-tetrad (Fig. 6A), *vs.* loop (Fig. 6B)). In contrast, the single-band emission exhibited by the vAcphdG probe resembled the emissive behaviour of stilbenes, in which D and A groups are separated by a vinyl linker.[51] For the stilbene class of molecular rotors the TICT energy gap is much smaller than the LE energy gap and relaxation from the TICT state occurs without photon emission. The emission of these probes increases with solvent viscosity because viscous solvents increase the energy barrier between the LE and TICT states. Molecular rotor probes that provide single-band emission are more useful for viscosity-sensing applications because their emission is relatively insensitive toward solvent polarity.[51] Therefore, vAcphdG is a much more useful viscosity-sensing nucleobase probe than AcphdG, as it is more emissive in water (Table 2), exhibits more red-shifted excitation and emission wavelengths in DNA (Table 4), is far less disturbing to duplex and GQ formation (Table 3) and provides single-band emission in mTBA that exhibits a correlation between emission intensity and solvent viscosity (Fig. 6C and D). These features should allow quantification of the micro-viscosity of the environment within oligonucleotides,[51] which can be a versatile tool for detecting specific biomolecular interactions.[52] Further optimization of viscosity-sensitive nucleobase probes structurally related to vAcphdG is currently underway for the development of fluorescent nucleobase mimics for monitoring specific oligonucleotide-protein interactions.

Experimental section

Materials

Boronic acids (benzo[*b*]thien-2-ylboronic acid, pyrene-1-boronic acid, 4-acetylphenylboronic acid, and 8-quinoline boronic acid), $Pd(OAc)_2$, 3,3′,3″-phosphanetriyltris (benzenesulfonic acid) trisodium salt (TPPTS), *N*,*N*-dimethyl-formamide diethyl acetal, 4,4′-dimethoxytrityl chloride, 2-cyanoethyl *N*,*N*-diisopropyl-chlorophosphoramidite, and other commercial products used for phosphoramidite synthesis were used as received. PEG-200 and PEG-600 were purchased from Sigma. Unmodified TBA oligonucleotides and complementary strands were purchased from Sigma Genosys and were purified by Sigma using polyacrylamide gel electrophoresis. All unmodified phosphoramidites (bz-dA-CE, ac-dC-CE, dmf-dG-CE and dT-CE), activator (0.25 M 5-(ethylthio)-1*H*-tetrazole in CH_3CN), oxidizing agent (0.02 M I_2 in THF/pyridine/H_2O, 70/20/10, v/v/v), deblock (3% dichloroacetic acid in dichloromethane), cap A (THF/2,6-lutidine/acetic anhydride),

cap B (methylimidazole in THF), and 1000 Å controlled pore glass (CPG) solid supports were purchased from BioAutomation or Glen Research.

Methods

NMR spectra were recorded at room temperature on 300, 400 and 600 MHz Bruker spectrometers in either $CDCl_3$, CD_2Cl_2 or DMSO-d_6 referenced to TMS (0 ppm) or the respective solvent. Full synthetic details of modified phosphoramidites, NMR spectra and ESI-MS analysis of modified *Nar*I oligonucleotides are available in the ESI.† The quantum yields of the 8aryldG probes were determined in 10 mM MOPS buffer (pH 7, 100 mM NaCl) using the comparative method. Quinine bisulfate (Φ_{fl} = 0.546 in 0.5 M H_2SO_4) served as the fluorescence quantum yield standard. High-resolution mass spectra were obtained with an Agilent LC-UHD quadrupole time-of-flight (Q-Tof) instrument using electrospray ionization. All mTBA oligonucleotides were prepared on a 1 μmol scale using a BioAutomation MerMade 12 automatic DNA synthesizer. Standard phosphoramidites were prepared in dry acetonitrile (1 mM) and coupling reactions consisted of a 70 μL injection volume with a 60 s coupling time. For modified phosphoramidites the injection volume from the 1 mM acetonitrile solutions was also 70 μL, but the coupling time was increased to 120 s. The crude mTBA oligonucleotide solutions were deprotected and cleaved from their solid support in aqueous ammonium hydroxide at 55 °C for 15 h, filtered using syringe filters (PVDF 0.22 μm) and concentrated under diminished pressure. Samples were then resuspended in Milli-Q water (18.2 MΩ) and purified using an Agilent HPLC instrument equipped with an autosampler, a diode array detector, fluorescence detector and autocollector. Separation was carried out at 50 °C using a 5 μm reversed-phase (RP) semi-preparative C18 column (100 × 10 mm) with a flow rate of 3.5 mL min^{-1}, and various gradients of buffer B in buffer A (buffer A = 95 : 5 aqueous 50 mM TEAA, pH 7.2/acetonitrile; buffer B = 30 : 70 aqueous 50 mM TEAA, pH 7.2/acetonitrile). Yields of the mTBA samples were estimated from integration of the semi-preparative HPLC trace. Following lyophilisation of the collected fractions, the mTBA samples were analyzed using analytical HPLC to check for purity. Analytical HPLC separation was performed using a Clarity Oligo-RP C18 column (4.6 mm × 50 mm, 3 μm, Phenomenex). Buffer A contained 100 mM TEAA (pH 7.2) and 5% CH_3CN (v/v). Buffer B contained 100 mM TEAA (pH 7.2) and 20% CH_3CN (v/v). The flow rate for this method was maintained at 0.5 mL min^{-1} using a multistep gradient protocol. From 0-3 min, hold A and B at 73 and 27% respectively. From 3–23 min, a linear program to 100% B; 23–25 min, hold at 100% B; 25–27 min linear program to 73 and 27% A and B respectively; 27–35 min hold at 73% A and 27% B for column equilibration. Integration of the analytical HPLC chromatograms indicated purity levels >85% for the mTBA samples.

MS experiments for identification of the mTBA oligonucleotides were conducted on a Bruker amaZon quadrupole ion trap SL spectrometer. Oligonucleotide samples were prepared in 90% Milli-Q filtered water/10% methanol containing 0.1 mM ammonium acetate. Masses were acquired in the negative ionization mode with an electrospray ionization source (see ESI† for MS spectra).

All melting temperatures (T_m) of TBA oligonucleotides were measured using a Cary 300-Bio UV-Vis spectrophotometer equipped with a 6 × 6 multicell Peltier block-heating unit using Hellma 114-QS 10 mm light path cells. Oligonucleotide samples were prepared in 50 mM phosphate buffer, pH 7, with 100 mM MCl (M = Na^+ or K^+), using equivalent amounts (6.0 μM) of the unmodified or 8-aryl-dG modified TBA oligonucleotide and its complementary strand. The UV absorption at 260 nm (for duplex formation) and 295 nm (for GQ formation) was monitored as a function of temperature and consisted of forward-reverse scans from 10 to 90 °C at a heating rate of 0.5 °C min^{-1}, which was repeated five times. The T_m values were determined using hyperchromicity calculations provided in the Thermal software.

Circular dichroism (CD) spectra were recorded on a Jasco J-815 CD spectropolarimeter equipped with a 1 x 6 Multicell block thermal controller and a water circulator unit. Spectra were collected at 10 °C between 200 and 400 nm, with a bandwidth of 1 nm and scanning speed at 100 nm min^{-1}, as previously described.[38] All fluorescence spectra were recorded on a Cary Eclipse Fluorescence spectrophotometer equipped with a 1 × 4 Multicell block Peltier stirrer and temperature controller. Excitation and emission spectra (5 nm slit-width) were recorded at 10 °C. Computational methods are available in the ESI,† and followed strategies previously outlined.[9,10]

Conclusions

These results demonstrate the fluorescence response of donor–acceptor (D–A) 8-aryl-dG probes within the thrombin binding aptamer (TBA). Probes with the 8-aryl moiety directly attached to the dG component are restricted to *syn*-positions within the G-tetrad of TBA, as they strongly destabilize the G-quadruplex (GQ) structure when placed in an *anti*-position. At the *syn*-G_5 position of TBA, it was found that the size of the 8-aryl moiety strongly influenced GQ stability, with AcphG > BthG > QG ≫ PyG. Compared to unmodified TBA, AcphG displayed a ΔT_m = +6.9 °C, while the ΔT_m was −15.3 °C for PyG. Probes with strong acceptor groups (*i.e.* 4-acetylphenyl) produced twisted charge transfer (CT_T) states and displayed quenched emission in water. Such probes were not particularly useful for distinguishing duplex from GQ structures in aqueous K^+ solution when inserted into a *syn*-position of the G-tetrad, because they exhibited quenched fluorescence in both duplex and GQ structures. However, the probes may be useful in the loop-G_8 position of TBA, because they displayed CT emission in the duplex (probe is flanked by two T bases) that was quenched in the GQ due to stacking interactions with the G-tetrad. When the 8-aryl moiety is separated from the dG component by a vinyl linker, the probes can be selectively excited at ~390 nm, which is far removed from the excitation wavelength of the natural DNA nucleobases. Depending on the nature of the 8-aryl group attached to the vinyl linker, the probe can be inserted into an *anti*-position

within the G-tetrad without perturbing the stability of the GQ structure. Overall, our studies demonstrated that D–A probes that favour (twisted) CT_T states are potentially useful for monitoring changes in emission intensity and wavelength in a crowded environment because the probes are effective molecular rotors with emission that responds to solvent viscosity. Probes that generate (planar) CT_P states can show visibly bright emission in both duplex and GQ structures in aqueous K^+ solutions. However, such probes exhibit emission that is less sensitive to viscosity and solvent polarity compared to D–A probes that generate CT_T states.

Acknowledgements

This work was supported by the Natural Sciences and Engineering Research Council of Canada (Discovery grants to R.A.M, 311600-2013, and S.D.W., 249598-07); and the Canada Research Chair Program (S.D.W., 950-228175). Computational resources provided by Westgrid and Compute/Calcul Canada are greatly appreciated.

Notes and references

1 J. N. Wilson and E. T. Kool, *Org. Biomol. Chem.*, 2006, **4**, 4265–4274.
2 D. W. Dodd and R. H. E. Hudson, *Mini-Rev. Org. Chem.*, 2009, **6**, 378–391.
3 L. M. Wilhelmsson, *Q. Rev. Biophys.*, 2010, **43**, 159–183.
4 R. W. Sinkeldam, N. J. Greco and Y. Tor, *Chem. Rev.*, 2010, **110**, 2579–2619.
5 N. J. Greco and Y. Tor, *J. Am. Chem. Soc.*, 2005, **127**, 10784–10785.
6 N. J. Greco and Y. Tor, *Tetrahedron*, 2007, **63**, 3515–3527.
7 R. W. Sinkeldam, A. J. Wheat, H. Boyaci and Y. Tor, *ChemPhysChem*, 2011, **12**, 567–570.
8 R. W. Sinkeldam, P. Marcus and D. Uchenik, and Y. Tor, *ChemPhysChem*, 2011, **12**, 2260–2265.
9 K. M. Rankin, M. Sproviero, K. Rankin, P. Sharma, S. D. Wetmore and R. A. Manderville, *J. Org. Chem.*, 2012, **77**, 10498–10508.
10 M. Sproviero, K. L. Fadock, A. A. Witham, R. A. Manderville, P. Sharma and S. D. Wetmore, *Chem. Sci.*, 2014, **5**, 788–796.
11 M. Sproviero and R. A. Manderville, *Chem. Commun.*, 2014, **50**, 3097–3099.
12 M. Sproviero, K. L. Fadock, A. A. Witham and R. A. Manderville, *ACS Chem. Biol.*, 2015, **10**, 1311–1318.
13 D. J. M. Blanchard, T. Z. Cservenyi and R. A. Manderville, *Chem. Commun.*, 2015, **51**, 16829–16831.
14 A. L. Millen, C. K. McLaughlin, K. M. Sun, R. A. Manderville and S. D. Wetmore, *J. Phys. Chem. A*, 2008, **112**, 3742–3753.
15 M. Sproviero, A. M. R. Verwey, K. M. Rankin, A. A. Witham, D. V. Soldatov, R. A. Manderville, M. I. Fekry, S. J. Sturla, P. Sharma and S. D. Wetmore, *Nucleic Acids Res.*, 2014, **42**, 13405–13421.
16 G. Biffi, D. Tannahill, J. McCafferty and S. Balasubramanian, *Nat. Chem.*, 2013, **5**, 182–186.
17 M. L. Bochman, K. Paeschke and V. A. Zakian, *Nat. Rev. Genet.*, 2012, **13**, 770–780.
18 G. W. Collie and G. N. Parkinson, *Chem. Soc. Rev.*, 2011, **40**, 5867–5892.
19 W. O. Tucker, K. T. Shum and J. A. Tanner, *Curr. Pharm. Des.*, 2012, **18**, 2014–2026.
20 D. D. Le, M. Di Antonio, L. K. M. Chan and S. Balasubramanian, *Chem. Commun.*, 2015, **51**, 8048–8050.
21 Y. Xu, Y. Suzuki, K. Ito and M. Komiyama, *Proc. Natl. Acad. Sci. U. S. A.*, 2010, **107**, 14579–14584.
22 J. Mohanty, N. Barooah, V. Dhamodharan, S. Harikrishna, P. I. Pradeepkumar and A. C. Bhasikuttan, *J. Am. Chem. Soc.*, 2013, **135**, 367–376.
23 A. Renaud de la Faverie, A. Guédin, A. Bedrat, L. A. Yatsunyk and J.-L. Mergny, *Nucleic Acids Res.*, 2014, **42**, e65.
24 D.-M. Kong, Y.-E. Ma, J. Wu and H.-X. Shen, *Chem. – Eur. J.*, 2009, **15**, 901–909.
25 R. W. Sinkeldam, P. A. Hopkins and Y. Tor, *ChemPhysChem*, 2012, **13**, 3350–3356.
26 P. A. Hopkins, R. W. Sinkeldam and Y. Tor, *Org. Lett.*, 2014, **16**, 5290–5293.
27 G. Mata and N. W. Luedtke, *Org. Lett.*, 2013, **15**, 2462–2465.
28 G. Mata and N. W. Luedtke, *J. Am. Chem. Soc.*, 2015, **137**, 699–707.
29 L. C. Bock, L. C. Griffin, J. A. Latham, E. H. Vermaas and J. J. Toole, *Nature*, 1992, **355**, 564–566.
30 B. Deng, Y. Lin, C. Wang, F. Li, Z. Wang and H. Zhang, *Anal. Chim. Acta*, 2014, **837**, 1–15.
31 R. S. Butler, P. Cohn, P. Tenzel, K. A. Abboud and R. K. Castellano, *J. Am. Chem. Soc.*, 2009, **131**, 623–633.
32 Y. Saito, A. Suzuki, K. Imai, N. Nemoto and I. Saito, *Tetrahedron Lett.*, 2010, **51**, 2606–2609.
33 Y. Saito, A. Suzuki, S. Ishioroshi and I. Saito, *Tetrahedron Lett.*, 2011, **52**, 4726–4729.
34 A. Dumas and N. W. Luedtke, *J. Am. Chem. Soc.*, 2010, **132**, 18004–18007.
35 M. Maus, W. Rettig, D. Bonafoux and R. Lapouyade, *J. Phys. Chem. A*, 1999, **103**, 3388–3401.
36 A. Maliakal, G. Lem, N. J. Turro, R. Ravichandran, J. C. Suhadolnik, A. D. DeBellis, M. G. Wood and J. Lau, *J. Phys. Chem. A*, 2002, **106**, 7680–7689.
37 L. Valis, E. Mayer-Enthart and H.-A. Wagenknecht, *Bioorg. Med. Chem. Lett.*, 2006, **16**, 3184–3187.
38 M. Sproviero, A. M. R. Verwey, A. A. Witham, R. A. Manderville, P. Sharma and S. D. Wetmore, *Chem. Res. Toxicol.*, 2015, **28**, 1647–1658.
39 A. Dumas and N. W. Luedtke, *Nucleic Acids Res.*, 2011, **39**, 6825–6834.
40 L. Gillet and O. D. Schärer, *Org. Lett.*, 2002, **4**, 4205–4208.
41 E. C. Western, J. R. Daft, E. M. Johnson II, P. M. Gannett and K. H. Shaughnessy, *J. Org. Chem.*, 2003, **68**, 6767–6774.
42 S. Ladouceur, A. M. Soliman and E. Zysman-Colman, *Synthesis*, 2011, 3604–3611.

43 Z.-C. Miao, D. Wang, Y.-M. Zhang, Z.-K. Jin, F. Liu, F.-F. Wang and H. Yang, *Liq. Cryst.*, 2012, **39**, 1291–1296.
44 R. Alfaro, A. Parra, J. Alemán, J. L. G. Ruano and M. Tortosa, *J. Am. Chem. Soc.*, 2012, **134**, 15165–15168.
45 Y. Saito, K. Matsumoto, Y. Takeuchi, S. S. Bag, S. Kodate and T. Morii, and I. Saito, *Tetrahedron Lett.*, 2009, **50**, 1403–1406.
46 D. M. Gray, R. L. Ratliff and M. R. Vaughan, *Methods Enzymol.*, 1992, **211**, 389–406.
47 A. Ambrus, D. Chen, J. Dai, T. Bialis and R. A. Jones D. Yang, *Nucleic Acids Res.*, 2006, **34**, 2723–2735.
48 M. C. Miller, R. Buscaglia, J. B. Chaires, A. N. Lane and J. O. Trent, *J. Am. Chem. Soc.*, 2010, **132**, 17105–17107.
49 B. Heddi and A. T. Phan, *J. Am. Chem. Soc.*, 2011, **133**, 9824–9833.
50 D. Miyoshi and N. Sugimoto, *Biochimie*, 2008, **90**, 1040–1051.
51 M. A. Haidekker and E. A. Theodorakis, *J. Biol. Eng.*, 2010, **4**, 11.
52 W. L. Goh, M. Y. Lee, T. L. Joseph, S. T. Quah, C. J. Brown, C. Verma, S. Brenner, F. J. Ghadessy and Y. N. Teo, *J. Am. Chem. Soc.*, 2014, **136**, 6159–6162.

